Performance Analysis of Parametric Channel Estimation for 3D Massive MIMO/FD-MIMO OFDM Systems.

By

Rubayet Shafin

Submitted to the Department of Electrical Engineering and Computer Science and the Graduate Faculty of the University of Kansas
in partial fulfillment of the requirements for the degree of
Masters of Science

Lingjia Liu, Chairperson

Committee members

Erik Perrins

Yang Yi

Date defended: April 25, 2017

The Thesis Committee for Rubayet Shafin certifies
that this is the approved version of the following thesis :

Performance Analysis of Parametric Channel Estimation for 3D Massive MIMO/FD-MIMO OFDM Systems.

Lingjia Liu, Chairperson

Date approved:

Abstract

With the promise of meeting future capacity demands for mobile broadband communications, 3D massive-MIMO/Full Dimension MIMO (FD-MIMO) systems have gained much interest among the researchers in recent years. Apart from the huge spectral efficiency gain offered by the system, the reason for this great interest can also be attributed to significant reduction of latency, simplified multiple access layer, and robustness to interference. However, in order to completely extract the benefits of massive-MIMO systems, accurate channel state information is very critical. In this paper, a channel estimation method based on direction of arrival (DoA) estimation is presented for massive-MIMO OFDM systems. To be specific, the DoA is estimated using Estimation of Signal Parameter via Rotational Invariance Technique (ESPRIT) method, and the root mean square error (RMSE) of the DoA estimation is analytically characterized for the corresponding MIMO-OFDM system.

Contents

List of Figures

Chapter 1

Introduction

Recently, massive-MIMO, also known as large-scale MIMO, has created much interests, both in academia and industry, with the promise of meeting future capacity demands by providing increased spectral-efficiency achieved through aggressive spatial multiplexing. Considering the form factor limitation at the base station (BS), instead of placing a large number of antennas horizontally, 3D massive-MIMO system employs those antennas in a 2D antenna array panel enabling the exploration of the degrees of freedom in elevation domain along with those in the azimuth domain. Accordingly, 3D massive-MIMO is also called as full-dimension MIMO (FD-MIMO) in 3GPP LTE-Advanced systems. Apart from the huge potential of providing excellent spatial resolution and array gains, massive-MIMO can also offer a significant reduction of latency, a simplified multiple access layer, and robustness to interference [Larsson et al., 2014]. With the help of a large number of antennas, this system can concentrate more energy in a particular direction leading to a dramatic increase in energy-efficiency. Furthermore, massive-MIMO is the key enabling technology for gigabit-per-second data transmission in the millimeter wave (mmW) wireless communications with carrier frequency between 30 and 300 GHz. In mmW communications, it becomes feasible to pack a greater number of antennas at the base station. However, the benefits of Massive MIMO are limited by the accuracy of the channel state information (CSI) obtained at the

transmitter. The CSI is critical for functionalities such as downlink beam-forming, transmit precoding, user scheduling, etc.

MIMO technology, together with Orthogonal Frequency Division Multiplexing (OFDM), offer efficient ways of increasing the spectral efficiency of the cellular system. The high-data-rate wireless transmission scheme, OFDM, converts a frequency-selective MIMO channel into a parallel collection of frequency-flat subchannels, which is beneficial for detection and channel estimation. It is shown in [Stuber et al., 2004] that unprecedented spectral efficiency and promising system throughput can be obtained through the combination of these two powerful technologies– MIMO and OFDM.

Because of the sensitivity of MIMO algorithms with respect to the underlying channel matrix, channel state information is particularly critical in order to assess the performance of the of underlying MIMO-OFDM systems. In general, channel matrix for MIMO systems can be modeled in different ways. The parametric channel model is adopted by performing virtual direction-of-arrival (DoA) and direction-of-departure (DoD) estimation of resolvable paths. It provides a simple geometric interpretation of the scattering environment in characterizing the two key MIMO channel metrics: ergodic capacity and diversity level [Sayeed & Sivanadyan, 2010]. Despite the advantage of reducing the number of estimation parameters, it is shown in [Larsen et al., 2009] that channel estimation based on DoA and DoD provides the best performance in terms of error bound.

In this paper, based on the parametric channel model, we present a DoA estimation method for massive-MIMO OFDM system using ESPRIT type algorithms, and analytically characterize the root mean square error (RMSE) of the elevation and azimuth angles for resolvable paths. From the results obtained, we try to deduce valuable intuition on real system design. Specifically, our results show that for the case of massive-MIMO OFDM systems, RMSE depends heavily on number of antennas, antenna orientation, number of snapshots, and correlation of the transmitted signal. The rest of the paper is organized as follows: The system model is introduced in Section II. The subsequent Section III presents

the ESPRIT-based DoA estimation algorithms for this MIMO-OFDM system. Analytical expression for the MSE of the DoA estimation is presented in Section IV. The simulation result is shown in Section V before drawing conclusion in Section VI.

Chapter 2

System Model

Consider a MIMO-OFDM system with N_t transmit antennas and N_r receive antennas. At each transmitter, the high-rate information symbols to be transmitted are grouped into blocks of length N_c. The i-th such block at the j_t-th transmitter can be represented as $\mathbf{x}_{i,j_t} = [x_{i,j_t}(0), x_{i,j_t}(1), \ldots, x_{i,j_t}(N_c - 1)]^T$, where $x_{i,j_t}(k)$ denotes the k-th information symbol within the i-th block at the j_t-th transmitter. After serial-to-parallel conversion, these discrete frequency components of the OFDM modulator are then converted into time samples by performing an inverse fast Fourier transform (IFFT). The IFFT operation yields the OFDM symbol consisting of the sequence $s_{i,j_t}(0), s_{i,j_t}(1), \ldots, s_{i,j_t}(N_c - 1)$, where $\{s_{i,j_t}(n)\}$ corresponds to the IFFT samples of the multi-carrier signal at the j_t-th transmitter, and can be written as

$$s_{i,j_t}(n) = \frac{1}{\sqrt{N_c}} \sum_{k=0}^{N_c-1} x_{i,j_t}(k) e^{j2\pi kn/N_c}, \quad 0 \leq n \leq N_c - 1. \tag{2.1}$$

The n-th samples at all the transmitters can be expressed in a vector form $\mathbf{s}_i(n) = [s_{i,j_0}(n), s_{i,j_1}(n), \ldots, s_{i,j_{(N_t-1)}}(n)]^T$. The cyclic prefix (CP) is also added to the OFDM symbol. In order to avoid inter-symbol interference (ISI), the length of the cyclic prefix should be no shorter than the channel length. After appending CP, the resulting sequence $\tilde{s}_{i,j_t}(n)$ is first passed through a parallel-to-serial converter followed by a digital-to-analog converter,

resulting in the baseband OFDM signal, $r(t)$. The baseband signal is then upconverted and sent through a frequency selective fading channel, which is assumed to remain time-invariant during one OFDM symbol duration. We assume that the channel, which can be represented by an equivalent discrete-time linear channel impulse response (CIR), has a finite number (L) of non-zero taps.

Traditional channel models such as Rayleigh Fading model, which depict rich scattering environment, do not really portray the actual scenario for millimeter wave wireless communication. In this paper, a clustered channel model is considered, where each scattering cluster is assumed to contribute a single propagation path. The channel impulse responses are then represented by a sequence of channel matrices, $\mathbf{C}(\ell)$ for $\ell = 0, 1, \ldots, (L-1)$. We assume there are a finite number of resolvable paths between the transmitter and receiver. For the broadband millimeter wave communication, we can consider that each channel tap corresponds to each path. The channel impulse response for the ℓ-th tap is given by

$$\mathbf{C}(\ell) = \alpha(\ell)\mathbf{e}_r(\ell)\mathbf{e}_t^H(\ell) \tag{2.2}$$

where $\alpha(\ell)$, $\mathbf{e}_r(\ell)$ and $\mathbf{e}_t(\ell)$ are, respectively, the channel gain, $N_r \times 1$ receive antenna array response and $N_t \times 1$ transmit antenna array response for the ℓ-th tap; $(.)^H$ denotes hermitian matrix. It is obvious that the transmit and receive antenna array responses depend on DoD and DoA respectively. For the transmitter equipped with a uniform linear array (ULA), the transmit antenna array response can be described using the Vandermonde structure: $\mathbf{e}_t(\ell) = \begin{bmatrix} 1 & e^{j\omega_\ell} & \ldots & e^{j(N_t-1)\omega_\ell} \end{bmatrix}^T$, where $\omega_\ell = (2\pi\Delta/\lambda)\cos\Omega_\ell$, Δ is the spacing between the adjacent transmit antenna elements, Ω_ℓ is the transmit angle (DoD) for the ℓ-th tap, and λ is the carrier wavelength.

The antenna array at the base station is a planar array placed in the X-Z plane, with M_1 and M_2 antenna elements in vertical and horizontal direction respectively (Fig. 2.1). Accordingly, the number of receive antenna elements at the base station is $N_r = M_1 M_2$.

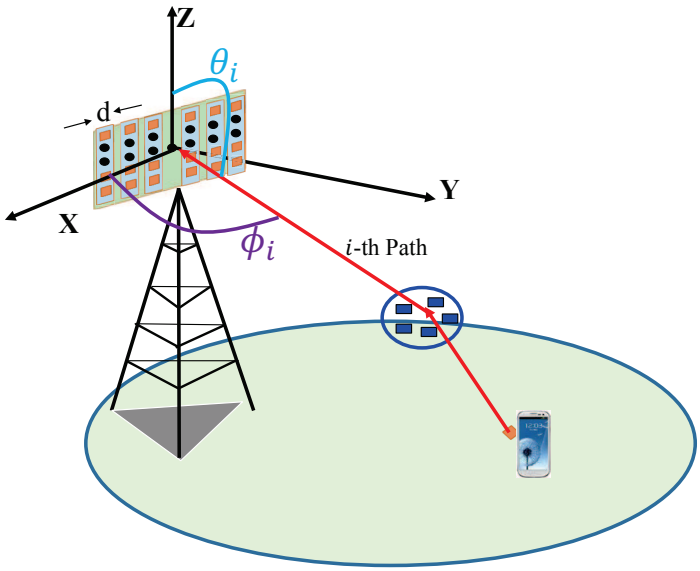

Figure 2.1: 3D Massive MIMO/FD-MIMO System Model.

Since the antenna elements at the base station are placed in a 2D plane, for each resolvable path, there will be an azimuth DoA and an elevation DoA. Therefore, the receive antenna array response can be expressed as $\mathbf{e}_r(\ell) = \mathbf{a}(v_\ell) \otimes \mathbf{a}(u_\ell)$, where $\otimes$ represents the Kronecker product. $\mathbf{a}(u_\ell) = \begin{bmatrix} 1 & e^{ju_\ell} & \dots & e^{j(M_1-1)u_\ell} \end{bmatrix}^T$ and $\mathbf{a}(v_\ell) = \begin{bmatrix} 1 & e^{jv_\ell} & \dots & e^{j(M_2-1)v_\ell} \end{bmatrix}^T$ can be viewed as the receive steering vectors of the elevation and azimuth angles respectively. Here, $u_\ell = \frac{2\pi d}{\lambda} \cos\theta_\ell$ and $v_\ell = \frac{2\pi d}{\lambda} \sin\theta_\ell \cos\phi_\ell$ are the two receive spatial frequencies at the base station, d is the spacing between adjacent antenna elements in the receive antenna array, and θ_ℓ and ϕ_ℓ is the elevation and azimuth DoA respectively.

At each receiver, the received signal is first down-converted, and then passed through a low-pass filter to remove the high frequency components. The received base-band signal at the j_r-th receiver, $y_{i,j_r}(t)$ is then passed through an analog-to-digital (A/D) converter. The cyclic prefix is then removed from the output of the A/D converter which yields the sequence $\mathbf{y}_i(n) = \mathbf{s}_i(n) \circledast \mathbf{C}(n) + \mathbf{w}_i(n)$, where $\circledast$ represents circular convolution, $\mathbf{y}_i(n) = [y_{i,j_0}(n), y_{i,j_1}(n), \dots, y_{i,j_{(N_r-1)}}(n)]^T$ is the vector containing n-th received sample at all the receiver, j_r represents the index for the receive antenna, and $\mathbf{w}_i(n)$ is the noise vector. It is to be noted here that $\mathbf{s}_i(n)$ has a sequence of length N_c, whereas, $\mathbf{C}(\ell)$ has sequence of

only length L. Therefore, for facilitating the circular convolution in the DFT operation, we append $(N_c - L)$ zero matrices to the sequence of $\mathbf{C}(\ell)$, so that both the channel impulse response and transmitted IFFT sample vector are of the same sequence-length, N_c. We can arrange the transmitted time-samples of the OFDM symbol in a tall $N_t N_c \times 1$ vector, $\tilde{\mathbf{s}}_i = \begin{bmatrix} \mathbf{s}_i^T(0) & \mathbf{s}_i^T(1) & \dots & \mathbf{s}_i^T(N_c-1) \end{bmatrix}^T$. For clarity, $\tilde{\mathbf{s}}_i$ can be expressed as $\tilde{\mathbf{s}}_i = \mathbf{F}\tilde{\mathbf{x}}_i$, where $\tilde{\mathbf{x}}_i$ is the corresponding $N_t N_c \times 1$ vector containing frequency-domain symbols, and $\mathbf{F}$ is the transformation matrix. Accordingly, we can represent the corresponding received N_c time-samples as $\tilde{\mathbf{y}}_i = \begin{bmatrix} \mathbf{y}_i^T(0) & \mathbf{y}_i^T(1) & \dots & \mathbf{y}_i^T(N_c-1) \end{bmatrix}^T$. We can thereby express the $N_r N_c \times 1$ received sample vector as

$$\tilde{\mathbf{y}}_i = \mathbf{C_c}\tilde{\mathbf{s}}_i + \tilde{\mathbf{w}}_i \tag{2.3}$$

where, $\tilde{\mathbf{w}}_i = \begin{bmatrix} \mathbf{w}_i^T(0) & \mathbf{w}_i^T(1) & \dots & \mathbf{w}_i^T(N_c-1) \end{bmatrix}^T$ is the $N_r N_c \times 1$ AWGN noise vector, and

$$\mathbf{C_c} = \begin{bmatrix} \mathbf{C}(0) & \mathbf{0} & \mathbf{0} & \dots & \mathbf{C}(1) \\ \mathbf{C}(1) & \mathbf{C}(0) & \mathbf{0} & \dots & \mathbf{C}(2) \\ & & \vdots & & \\ \mathbf{0} & \mathbf{0} & \mathbf{0} & \dots & \mathbf{C}(0) \end{bmatrix} \tag{2.4}$$

is the $N_r N_c \times N_t N_c$ block-circulant matrix governing the circular convolution.Therefore, the n-th received time-samples vector can be written as

$$\begin{aligned} \mathbf{y}(n) = &\mathbf{C}(n)\mathbf{s}(0) + \quad \mathbf{C}(n-1)\mathbf{s}(1) + \quad \dots \\ &\dots + \mathbf{C}(n - N_c + 1)\mathbf{s}(N_c - 1) + \mathbf{w}(n) \end{aligned} \tag{2.5}$$

where, $\mathbf{C}(\ell) = \mathbf{0}_{N_r \times N_t}$ for $L \leq \ell \leq (N_c - 1)$. It is to be noted here that we have dropped the index, i in (2.5) for notational convenience. It will be assumed from now on that all the samples correspond to i-th OFDM symbol. Using (2.2), and after a rearrangement, we can

write (2.5) as

$$\mathbf{y}(n) = \mathbf{A}\text{diag}\{\mathbf{b}\}\tilde{\mathbf{E}}_t\tilde{\mathbf{s}} + \mathbf{w}(n) \tag{2.6}$$

where, $\mathbf{A} = \begin{bmatrix}\mathbf{e}_r(n) & \mathbf{e}_r(n-1) & \dots & \mathbf{e}_r(n-N_c+1)\end{bmatrix}$ can be viewed as the array steering matrix, $\tilde{\mathbf{E}}_t$ is a $N_c \times N_t N_c$ block diagonal matrix containing the transmit array responses,

$$\tilde{\mathbf{E}}_t = \begin{bmatrix} \mathbf{e}_t^H(n) & \mathbf{0} & \dots & \mathbf{0} \\ \mathbf{0} & \mathbf{e}_t^H(n-1) & \dots & \mathbf{0} \\ & & \vdots & \\ \mathbf{0} & \mathbf{0} & \dots & \mathbf{e}_t^H(n-N_c+1) \end{bmatrix}, \tag{2.7}$$

and $\mathbf{b}$ is the $1 \times N_c$ row vector containing the the complex fading envelopes. Now, taking V snapshots during one IFFT-sample-duration, we can extend (2.6), and write as:

$$\mathbf{Y} = \mathbf{A}\text{diag}\{\mathbf{b}\}\tilde{\mathbf{E}}_t\tilde{\mathbf{S}} + \mathbf{W}, \tag{2.8}$$

where, $\mathbf{Y}$ is the $N_r \times V$ received signal at the base-station, $\tilde{\mathbf{S}}$ is the $N_t N_c \times V$ transmitted signal, and $\mathbf{W}$ is the $N_r \times V$ noise matrix. If the raised-cosine or square-root-raised-cosine functions are used for pulse shaping in the OFDM modulator, and uniform sampling is applied, $\tilde{\mathbf{S}}$ can be expressed as $\tilde{\mathbf{S}} = \tilde{\mathbf{s}}\mathbf{g}$, where, $\mathbf{g} = [g_1, g_2, \dots, g_V]$ is the $1 \times V$ row vector containing the snapshot-weights, which are the numbers with which if $\tilde{\mathbf{s}}$ is multiplied, corresponding snapshots can be determined. These weights are calculated by the number of snapshots and the parameters of the pulse shaping function. We can assume $\tilde{\mathbf{S}}^H\tilde{\mathbf{S}}$ to be a scaled identity matrix, which leads to the minimized channel estimation error. Moreover, if the optimal training sequence, such as Frank-Zadoff-Chu-sequences is used, we can still have the white Gaussian noise after the least-square channel estimation.

Chapter 3

DoA Estimation Through ESPRIT Algorithm

In this section, we introduce a low-complexity DoA estimation algorithm based on unitary ESPRIT in order to jointly estimate the elevation and azimuth angles. By converting all the complex matrices to the real matrices, the unitary ESPRIT performs the computations in real instead of complex numbers from beginning to the end of the algorithm, and hence reduces the computational complexity significantly. We can write the noisy received signal in (2.8) as:

$$\mathbf{Y} = \mathbf{AS} + \mathbf{W}, \tag{3.1}$$

where, $\mathbf{S} = \text{diag}\{\mathbf{b}\}\tilde{\mathbf{E}}_t\tilde{\mathbf{S}}$ can be regarded as the equivalent transmit signal. In order to perform the unitary ESPRIT, we need to use forward-backward averaging for processing the received signal:

$$\begin{aligned}\mathbf{Y}^{fba} &= \begin{bmatrix}\mathbf{Y} & \mathbf{\Pi}_{N_r}\mathbf{Y}\mathbf{\Pi}_V\end{bmatrix} \\ &= \begin{bmatrix}\mathbf{AS} & \mathbf{\Pi}_{N_r}\mathbf{A}^*\mathbf{S}^*\mathbf{\Pi}_V\end{bmatrix} + \begin{bmatrix}\mathbf{W} & \mathbf{\Pi}_{N_r}\mathbf{W}^*\mathbf{\Pi}_V\end{bmatrix}\end{aligned}$$

Here, $\mathbf{\Pi}_p$ denotes the $p \times p$ exchange matrix with ones on its antidiagonal and zeros elsewhere. The subspace decomposition of the signal space of the received signal through singular value decomposition then can be written as:

$$\begin{bmatrix} \mathbf{AS} & \mathbf{\Pi}_{N_r}\mathbf{A}^*\mathbf{S}^*\mathbf{\Pi}_V \end{bmatrix} = \begin{bmatrix} \mathbf{U}_s & \mathbf{U}_n \end{bmatrix} \begin{bmatrix} \mathbf{\Sigma}_s & \mathbf{0} \\ \mathbf{0} & \mathbf{0} \end{bmatrix} \begin{bmatrix} \mathbf{V}_s^H \\ \mathbf{V}_n^H \end{bmatrix} \tag{3.2}$$

The array manifold matrix of an $M_1 \times M_2$ rectangular antenna array can be expressed as:

$$\mathbf{A}(u_\ell, v_\ell) = \mathbf{a}(u_\ell)\mathbf{a}^T(v_\ell),$$

that is, the 2D steering matrix can be decomposed into product of two 1D steering vectors [Mathews et al., 1996]. We can choose the two subarrays of the steering vector, $\mathbf{a}(u_\ell)$, with maximum overlap, that is, each having $M_1 - 1$ antenna elements. Because of the fixed displacement between the first and second subarrays, if the first $M_1 - 1$ elements are multiplied by e^{ju_ℓ}, the resulting vector will be equal to the vector containing the last $M_1 - 1$ components. This can be expressed as:

$$e^{ju_\ell}\mathbf{J_1}\mathbf{a}(u_\ell) = \mathbf{J_2}\mathbf{a}(u_\ell), \tag{3.3}$$

where, $\mathbf{J_1}$ is an $(M_1 - 1) \times M_1$ selection matrix constructed by taking the first $(M_1 - 1)$ rows of $\mathbf{I}_{M_1}$ ($M_1 \times M_1$ Identity Matrix), and $\mathbf{J_2}$ is an $(M_1 - 1) \times M_1$ selection matrix constructed by taking the last $(M_1 - 1)$ rows of $\mathbf{I}_{M_1}$. A unitary and left-$\mathbf{\Pi}$ real matrix, $\mathbf{Q}_{M_1}$ can be constructed to change $\mathbf{a}(u_\ell)$ to a real-valued transformed steering vector, $\mathbf{a}^R(u_\ell)$,

$$\mathbf{a}^R(u_\ell) = \mathbf{Q}_{M_1}^H\mathbf{a}(u_\ell). \tag{3.4}$$

Assuming $M_1 = 2K$, $\mathbf{Q}_{M_1}$ can be constructed as

$$\mathbf{Q}_{2K} = \frac{1}{\sqrt{2}} \begin{bmatrix} \mathbf{I}_K & j\mathbf{I}_K \\ \mathbf{\Pi}_K & j\mathbf{\Pi}_K \end{bmatrix}, \tag{3.5}$$

where, $\mathbf{I}_K$ is a $K \times K$ identity matrix, and $\mathbf{\Pi}_K$ is a $K \times K$ exchange matrix.

Following our line of work [Wang et al., 2012], we have achieved the following relation:

$$\tan(\frac{u_\ell}{2})\mathbf{K}_1\mathbf{a}^R(u_\ell) = \mathbf{K}_2\mathbf{a}^R(u_\ell).$$

Here, $\mathbf{K}_1 = \mathrm{Re}\{\mathbf{Q}_{M_1-1}^H\mathbf{J}_2\mathbf{Q}_{M_1}\}$, $\mathbf{K}_2 = \mathrm{Im}\{\mathbf{Q}_{M_1-1}^H\mathbf{J}_2\mathbf{Q}_{M_1}\}$. Extending the relation to 2D antenna array:

$$\tan\left(\frac{u_\ell}{2}\right)\mathbf{K}_1\mathbf{A}^R(u_\ell, v_\ell) = \mathbf{K}_2\mathbf{A}^R(u_\ell, v_\ell), \tag{3.6}$$

where,

$$\mathbf{A}^R(u_\ell, v_\ell) = \mathbf{Q}_{M_1}^H\mathbf{a}(u_\ell)\mathbf{a}^T(v_\ell)\mathbf{Q}_{M_2}^* = \mathbf{a}^R(u_\ell)(\mathbf{a}^R(v_\ell))^T.$$

Furthermore, we can rewrite the formulation in (3.6) as:

$$\tan\left(\frac{u_\ell}{2}\right)\mathbf{K}_{x1}\mathrm{vec}\left\{\mathbf{A}^R(u_\ell, v_\ell)\right\} = \mathbf{K}_{x2}\mathrm{vec}\left\{\mathbf{A}^R(u_\ell, v_\ell)\right\}$$

where $\mathbf{K}_{x1} \triangleq \mathbf{I}_{M_2} \otimes \mathbf{K}_1$, $\mathbf{K}_{x2} \triangleq \mathbf{I}_{M_2} \otimes \mathbf{K}_2$, and vec$\{.\}$ is the vectorization operation. Accordingly, we can specify an $M_1M_2 \times N_c$ real-valued array manifold matrix:

$$\mathbf{A}^R \triangleq \left[\mathrm{vec}\left\{\mathbf{a}^R(u_n, v_n)\right\}, \ldots, \mathrm{vec}\left\{\mathbf{a}^R(u_{(n-N_c+1)}, v_{(n-N_c+1)})\right\}\right]$$

Then, we have the shift-invariance equation:

$$\mathbf{K}_{x1}\mathbf{A}^R\mathbf{\Omega}_x = \mathbf{K}_{x2}\mathbf{A}^R \tag{3.7}$$

where,

$$\mathbf{\Omega}_x \triangleq \text{diag}\left\{\tan\left(\frac{u_n}{2}\right), \tan\left(\frac{u_{n-1}}{2}\right), \ldots, \tan\left(\frac{u_{n-N_c+1}}{2}\right)\right\} \tag{3.8}$$

It is important to note that after the unitary transformation, the matrices all become real-valued matrices. This will significantly reduce the computational complexity.

Similarly, for $\mathbf{a}(v_\ell)$, we can conduct the same process. Let $\mathbf{K}_3 = \text{Re}\left\{\mathbf{Q}_{M_2-1}^H \mathbf{J}_2' \mathbf{Q}_{M_2}\right\}$, and $\mathbf{K}_4 = \text{Im}\left\{\mathbf{Q}_{M_2-1}^H \mathbf{J}_2' \mathbf{Q}_{M_2}\right\}$, where $\mathbf{J}_2'$ is the $(M_2-1)\times M_2$ matrix constructed by taking the last (M_2-1) rows of $\mathbf{I}_{M_2}$. Accordingly, we have

$$\mathbf{K}_{y1}\mathbf{A}^R\mathbf{\Omega}_y = \mathbf{K}_{y2}\mathbf{A}^R \tag{3.9}$$

where $\mathbf{K}_{y1} \triangleq \mathbf{K}_3 \otimes \mathbf{I}_{M_1}$, $\mathbf{K}_{y2} \triangleq \mathbf{K}_4 \otimes \mathbf{I}_{M_1}$, and

$$\mathbf{\Omega}_y \triangleq \text{diag}\left\{\tan\left(\frac{v_n}{2}\right), \tan\left(\frac{v_{n-1}}{2}\right), \ldots, \tan\left(\frac{v_{n-N_c+1}}{2}\right)\right\}$$

Let $\mathbf{U}_s$ be the signal subspace and $\mathbf{T}$ be the nonsingular transformation matrix, we have $\mathbf{U}_s = \mathbf{A}^R\mathbf{T}$ since the array steering matrix $\mathbf{A}^R$ and the matrix $\mathbf{U}_s$ span the same column space in the absence of noise or with an infinite number of measurements. Under the noisy case or with a finite number of measurements, this expression holds approximately [Haardt et al., 2008]. Substitute this relation into (3.7), we have

$$\mathbf{K}_{x1}\mathbf{U}_s\mathbf{\Psi}_x = \mathbf{K}_{x2}\mathbf{U}_s \tag{3.10}$$

where $\mathbf{\Psi}_x \triangleq \mathbf{T}^{-1}\mathbf{\Omega}_x\mathbf{T}$. Similarly, we also have

$$\mathbf{K}_{y1}\mathbf{U}_s\mathbf{\Psi}_y = \mathbf{K}_{y2}\mathbf{U}_s \tag{3.11}$$

where $\mathbf{\Psi}_y \triangleq \mathbf{T}^{-1}\mathbf{\Omega}_y\mathbf{T}$. From (3.10) and (3.11), we can solve for $\hat{\mathbf{\Psi}}_x$ and $\hat{\mathbf{\Psi}}_y$ based on the

estimated signal subspace using least square type of methods. Let the eigenvalues of the $N_c \times N_c$ complex matrix $\hat{\mathbf{\Psi}}_x + j\hat{\mathbf{\Psi}}_y$ be $\hat{\lambda}_\ell, \ell = 1, 2, \ldots, N_c$. u_ℓ and v_ℓ can be estimated from:

$$\hat{u}_\ell = 2\tan^{-1}\left\{\mathrm{Re}\left(\hat{\lambda}_\ell\right)\right\} \quad \hat{v}_\ell = 2\tan^{-1}\left\{\mathrm{Im}\left(\hat{\lambda}_\ell\right)\right\}$$

Accordingly, 2D DoAs of interest are obtained through simple parameter transformation.

Chapter 4

MSE Characterization

In this section, we present the theoretical analysis of root mean square error (RMSE) for DoA estimation using the standard ESPRIT method. Let $\hat{v}_\ell$ denote the estimated spatial frequency for ℓ-th tap; the estimation error is then given by $\Delta v_\ell = v_\ell - \hat{v}_\ell$. Similarly, $\Delta u_\ell = u_\ell - \hat{u}_\ell$. The first order approximation of the mean square estimation error of v_ℓ for the standard ESPRIT is given by [Roemer et al., 2014]:

$$E\{(\Delta v_\ell)^2\} = \frac{1}{2}\left(\mathbf{r}_\ell^{(v)H}\mathbf{W}_{mat}^{*}\mathbf{R}_{nn}^{T}\mathbf{W}_{mat}^{T}\mathbf{r}_\ell^{(v)} - Re\left\{\mathbf{r}_\ell^{(v)T}\mathbf{W}_{mat}\mathbf{C}_{nn}\mathbf{W}_{mat}^{T}\mathbf{r}_\ell^{(v)}\right\}\right), \tag{4.1}$$

where

$$\mathbf{r}_\ell^{(v)} = \mathbf{q}_\ell \otimes \left(\left[(\tilde{\mathbf{J}}_1^{(v)}\mathbf{U}_s)^{+}(\tilde{\mathbf{J}}_2^{(v)}/e^{jv_\ell} - \tilde{\mathbf{J}}_1^{(v)})\right]^T \mathbf{p}_\ell\right), \tag{4.2}$$

$$\mathbf{W}_{mat} = (\mathbf{\Sigma}_s^{-1}\mathbf{V}_s^T) \otimes (\mathbf{U}_n\mathbf{U}_n^H). \tag{4.3}$$

Here, $\tilde{\mathbf{J}}_1^{(v)}$ and $\tilde{\mathbf{J}}_2^{(v)}$ are the two effective selection matrices for the first and second subarrays, respectively, for the spatial frequency v_ℓ, $\mathbf{T}$ is the transformation matrix as described in Section II, $\mathbf{q}_\ell$ is the ℓ-th column of matrix $\mathbf{T}$, $\mathbf{p}_\ell^T$ is the ℓ-th row of matrix $\mathbf{T}^{-1}$; $\mathbf{R}_{nn}$ and $\mathbf{C}_{nn}$ are the covariance and complementary covariance matrices of the noise, respectively.

Similarly, we have

$$E\{(\Delta u_\ell)^2\} = \frac{1}{2}\left(\mathbf{r}_\ell^{(u)H}\mathbf{W}_{mat}^{*}\mathbf{R}_{nn}^{T}\mathbf{W}_{mat}^{T}\mathbf{r}_\ell^{(u)} - Re\left\{\mathbf{r}_\ell^{(u)T}\mathbf{W}_{mat}\mathbf{C}_{nn}\mathbf{W}_{mat}^{T}\mathbf{r}_\ell^{(u)}\right\}\right), \tag{4.4}$$

where

$$\mathbf{r}_\ell^{(u)} = \mathbf{q}_\ell \otimes \left(\left[(\tilde{\mathbf{J}}_1^{(u)}\mathbf{U}_s)^{+}(\tilde{\mathbf{J}}_2^{(u)}/e^{ju_\ell} - \tilde{\mathbf{J}}_1^{(u)})\right]^T \mathbf{p}_\ell\right). \tag{4.5}$$

Here, $\tilde{\mathbf{J}}_1^{(u)}$ and $\tilde{\mathbf{J}}_2^{(u)}$ are the two effective selection matrices for the first and second subarrays, respectively, for the spatial frequency u_ℓ. At this point, in order to facilitate the derivation of MSE expression, we consider the following Lemma:

Lemma 1. *If the elevation and azimuth angles are both drawn independently from a continuous distribution, the normalized array response vectors become orthogonal asymptotically, that is,* $\bar{\mathbf{e}}_r(k) \perp \boldsymbol{span}\{\bar{\mathbf{e}}_r(\ell) \mid \forall k \neq \ell\}$ *when the number of antennas at the base station goes large.*

Proof. See Appendix A.1. □

It is to be emphasized here that Lemma-1 holds for any continuous distribution. It can be seen that (4.1) depends on the singular value decomposition (SVD) of the noiseless received signal, which is not easy to obtain at the base station. In fact, it is extremely difficult to simplify such complicated result in the multiple path case. Fortunately, in the massive MIMO system, it can be significantly simplified because of the orthogonality of the steering vectors. The simplified result is only related to the real system parameters such as the number of antennas, number of snapshots, transmit power, and covariance matrix of transmit signal. Specifically, for the massive MIMO system, we have the following theorem:

Theorem 1. *For the case of 3D DoA estimation based on uniform rectangular array of* $M_1 \times M_2$ *elements, the root mean square errors of the elevation and azimuth angle estimations*

are given, respectively, by:

$$RMSE\{\theta_\ell\} = \frac{\sigma}{\pi \sin(\theta_\ell)(M_1 - 1)} \sqrt{\frac{\mathbf{R}_{SS}^{-1}(\ell,\ell)}{V M_2}} \tag{4.6}$$

$$RMSE\{\phi_\ell\} = \frac{\sigma}{\pi \sin(\theta_\ell)} \sqrt{\frac{\mathbf{R}_{SS}^{-1}(\ell,\ell)}{V}} \sqrt{\left(\frac{\cot^2(\theta_\ell)\cot^2(\phi_\ell)}{(M_1-1)^2 M_2} + \frac{1}{\sin^2(\phi_\ell)(M_2-1)^2 M_1} \right)} \tag{4.7}$$

where σ^2 is the noise variance, and $\mathbf{R}_{SS}(\ell,\ell)$ is the ℓ-th diagonal element of the covariance matrix of the equivalent transmit signal.

Proof. See Appendix A.2. □

Now, $\mathbf{R}_{SS} = \mathbb{E}\{\mathbf{S}\mathbf{S}^H\}/V$, where the expectation is with respect to the time-samples over different subcarriers on transmit antennas. $\mathbf{R}_{SS}$ can be expressed as:

$$\begin{aligned} \mathbf{R}_{SS} &= \text{diag}\{\mathbf{b}\}\tilde{\mathbf{E}}_t \mathbb{E}\{\tilde{\mathbf{S}}\tilde{\mathbf{S}}^H\}\tilde{\mathbf{E}}_t^H (\text{diag}\{\mathbf{b}\})^H / V \\ &= \text{diag}\{\mathbf{b}\}\tilde{\mathbf{E}}_t \mathbf{F} \mathbb{E}\{\tilde{\mathbf{X}}\tilde{\mathbf{X}}^H\}\mathbf{F}^H \tilde{\mathbf{E}}_t^H (\text{diag}\{\mathbf{b}\})^H / V \end{aligned} \tag{4.8}$$

where $\tilde{\mathbf{X}} = \mathbf{F}^{-1}\tilde{\mathbf{S}}$ is the frequency domain transmit signal matrix. If we assume, $\mathbf{Z} = \text{diag}\{\mathbf{b}\}\tilde{\mathbf{E}}_t\mathbf{F}$, we can write, $\mathbf{R}_{SS} = \mathbf{Z}\mathbb{E}\{\tilde{\mathbf{X}}\tilde{\mathbf{X}}^H\}\mathbf{Z}^H/V = \mathbf{Z}\mathbf{R}_{\tilde{\mathbf{X}}\tilde{\mathbf{X}}}\mathbf{Z}^H/V$, where $\mathbf{R}_{\tilde{\mathbf{X}}\tilde{\mathbf{X}}} = \mathbb{E}\{\tilde{\mathbf{X}}\tilde{\mathbf{X}}^H\}$. Therefore, we can write, $\mathbf{R}_{SS}^{-1} = (V)\mathbf{Z}^{-H}\mathbf{R}_{\tilde{\mathbf{X}}\tilde{\mathbf{X}}}^{-1}\mathbf{Z}^{-1}$. Plugging the expression for $\mathbf{R}_{SS}^{-1}$ in (4.6) and (4.7), we can obtain:

$$\text{RMSE}\{\theta_\ell\} = \frac{\sigma}{\pi \sin(\theta_\ell)(M_1 - 1)} \sqrt{\frac{(\mathbf{Z}^{-H}\mathbf{R}_{\tilde{\mathbf{X}}\tilde{\mathbf{X}}}^{-1}\mathbf{Z}^{-1})(\ell,\ell)}{M_2}} \tag{4.9}$$

$$\text{RMSE}\{\phi_\ell\} = \frac{\sigma}{\pi \sin(\theta_\ell)} \sqrt{(\mathbf{Z}^{-H}\mathbf{R}_{\tilde{\mathbf{X}}\tilde{\mathbf{X}}}^{-1}\mathbf{Z}^{-1})(\ell,\ell)} \sqrt{\left(\frac{\cot^2(\theta_\ell)\cot^2(\phi_\ell)}{(M_1-1)^2 M_2} + \frac{1}{\sin^2(\phi_\ell)(M_2-1)^2 M_1} \right)} \tag{4.10}$$

where $(\mathbf{Z}^{-H}\mathbf{R}^{-1}_{\tilde{\mathbf{X}}\tilde{\mathbf{X}}}\mathbf{Z}^{-1})(\ell,\ell)$ represents the ℓ-th diagonal element of the matrix product $\mathbf{Z}^{-H}\mathbf{R}^{-1}_{\tilde{\mathbf{X}}\tilde{\mathbf{X}}}\mathbf{Z}^{-1}$. Based on the proof of **Theorem 1**, it is straight forward to obtain the RMSE of the spatial frequencies u_ℓ and v_ℓ as follows:

Corollary 1. *In massive MIMO system, RMSEs of the spatial frequencies u_ℓ and v_ℓ using standard ESPRIT are given by:*

$$RMSE\{u_\ell\} = \frac{\sigma}{(M_1-1)}\sqrt{\frac{(\mathbf{Z}^{-H}\mathbf{R}^{-1}_{\tilde{\mathbf{X}}\tilde{\mathbf{X}}}\mathbf{Z}^{-1})(\ell,\ell)}{M_2}}, \tag{4.11}$$

$$RMSE\{v_\ell\} = \frac{\sigma}{(M_2-1)}\sqrt{\frac{(\mathbf{Z}^{-H}\mathbf{R}^{-1}_{\tilde{\mathbf{X}}\tilde{\mathbf{X}}}\mathbf{Z}^{-1})(\ell,\ell)}{M_1}}. \tag{4.12}$$

It is clear from these equations that correlation between the data on different subcarriers will have adverse effect on the performance of the DoA estimation, i.e., root mean squared error increases as the correlation between the data increases. The pilot sequence design will also have a significant impact on the DoA estimation performance through the term $\mathbf{R}_{\tilde{\mathbf{X}}\tilde{\mathbf{X}}}$.

Chapter 5

Simulation Results

In this section, we evaluate the RMSE of the ESPRIT-based DoA estimation for 3D millimeter wave massive MIMO systems. Furthermore, we will evaluate the system achievable rate under the presence of DoA estimation errors and present a performance comparison between our proposed power allocation algorithm and the traditional water-filling solution. To evaluate the performance of the DoA estimation, we assume there are 4 resolvable paths, which is a typical number for the outdoor millimeter-wave communication systems at both 28GHz and 73GHz [Rangan et al., 2014]. Number of subcarriers of the OFDM system is 32, and the length of cyclic prefix is 4. The antenna spacing for both the received and transmit antennas is assumed to be 0.5λ. The number of transmit antennas is set to be 8. The elevation and azimuth DoAs are chosen randomly from either the uniform distribution: $U[-180°, 180°]$, the exponential distribution: $Exp(1/50)$, or the Gaussian distribution: $\mathcal{N}(50, 20)$.

In our work, we invoke the far field assumption, and the wavefront impinging on the antenna array was assumed to be planer. However, using models such as Costa model, it would not be difficult to extend our results to incorporate the spherical wavefront. It is also noteworthy here that the transmission medium assumed in this paper is isotropic and linear. Normally distributed random numbers were used for generating frequency domain data for simulation. The number of snapshots is taken to be 32. The success of ESPRIT type high

resolution DoA estimation method depends on the full rank condition of the data covariance matrix. However, if appropriate preprocessing schemes such as forward-backward averaging or spatial smoothing can be applied, the data covariance matrix can be ensured to be of full rank and non-singular even when all the data signals are correlated. This is the main reason why we performed the forward-backward averaging in our DoA estimation process in Section II to deal with the potential issue of not having enough independent realizations of the random wavefield. Therefore, even though we used independent data signals in our simulation evaluation, our method/simulation procedure is expected to handle the non-singular covariance matrix case smoothly. The main requirement for forward-backward averaging to be valid is that the properties of the process under consideration be approximately the same independent of the orientation of space axis and that the samples be taken in a geometry that is also reversible. The antenna array that we are using at the base station fulfills this condition since it has a centro-symmetric structure. For the forward-backward averaging, the data are first taken from the 2D rectangular array, and then these data are vectorized. Finally, an extended data matrix is used for forward-backward averaging which is defined in Equation (**??**). Through forward-backward averaging, the data is effectively doubled to improve the estimation performance. Finally, the total available transmit power is assumed to be unity, and the SNR is defined as the ratio of the received signal power to the noise power, i.e. $\text{SNR} = 10\log_{10}(1/\sigma^2)$.

The performance of the estimation of elevation and azimuth angles for an 8×8 antenna array with uniform DoA distribution is shown in Figure 5.1 and Figure 5.2, respectively, where the analytical results for RMSEs are compared with the empirical ones. It can be observed that as SNR increases, the empirical results match the analytical results asymptotically. We can investigate the impact of various antenna configurations on the estimation performance and obtain some interesting design intuitions. For example, for a 3D massive MIMO system with the same total 64 antenna elements, the RMSE for 4×16 antenna array is shown in Figure 5.3 and Figure 5.4, while the elevation and azimuth angle estimation for

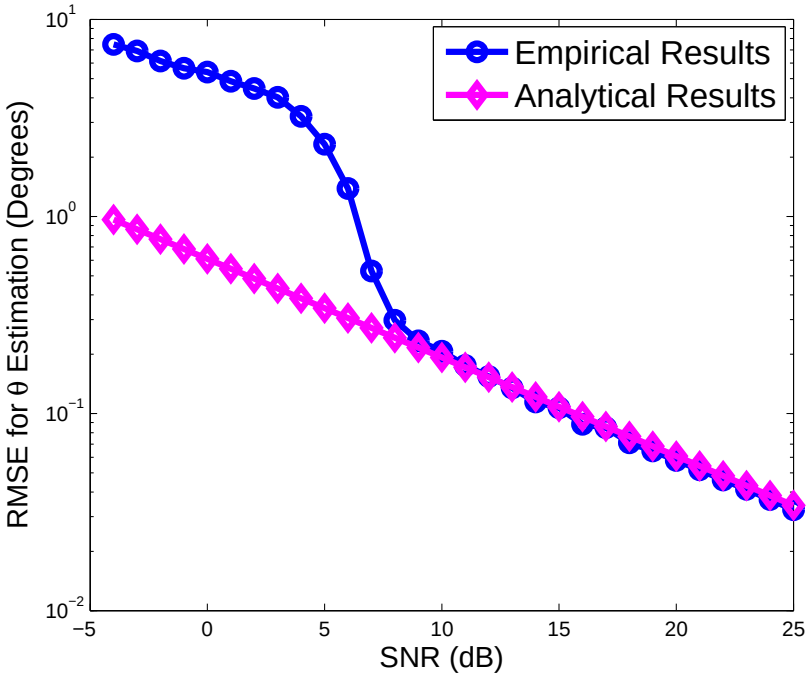

Figure 5.1: Elevation angle estimation for 8×8 array (Uniform DoA distribution).

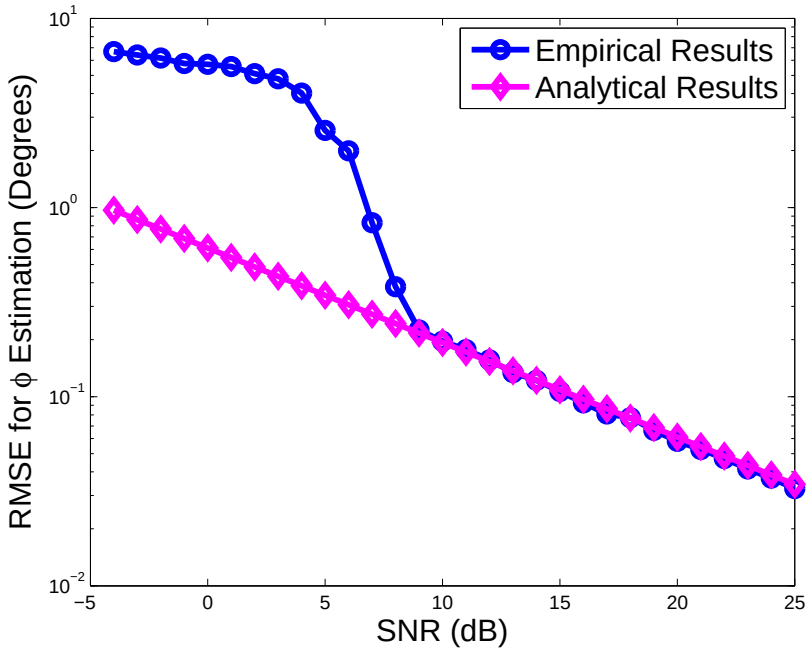

Figure 5.2: Azimuth angle estimation for 8×8 array (Uniform DoA distribution).

a 16×4 array are shown in Figure 5.5 and Figure 5.6, respectively. Comparing these figures with Figure 5.1 and 5.2, we observe that as the number of antennas in the elevation do-

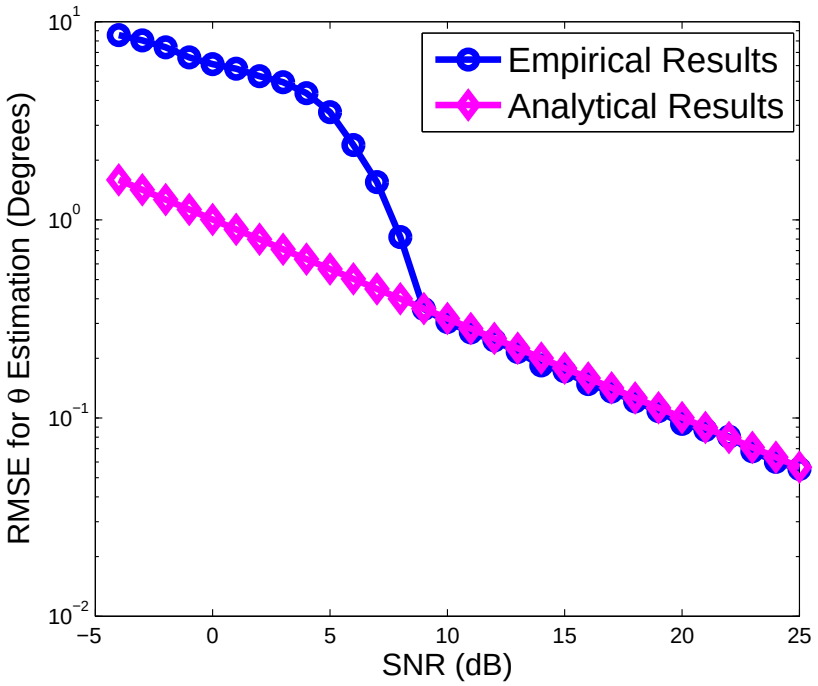

Figure 5.3: Elevation angle estimation for 4×16 array (Uniform DoA distribution).

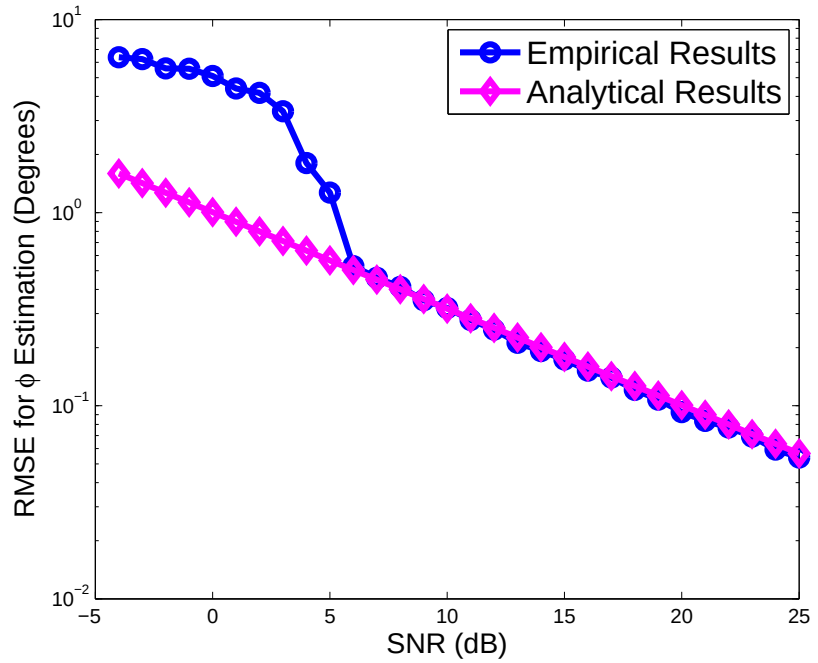

Figure 5.4: Azimuth angle estimation for 4×16 array (Uniform DoA distribution).

main increases, the elevation angle estimation performance improves. However, the RMSE of azimuth estimation of an 8×8 array shown in Figure 5.2 is even better than that of

the 4×16 array shown in Figure 5.4, especially at low and medium SNR regime. This is somewhat surprising because 4×16 array has more antenna elements in the azimuth domain compared with the 8×8 array. The reason behind this is that the azimuth estimation is actually coupled with the elevation estimation performance, and when the elevation estimation performance decreases, azimuth estimation performance also deteriorates even though the number of horizontal antennas is increased. On the other hand, the elevation angle estimation performance does not depend on the azimuth angle estimation performance. For

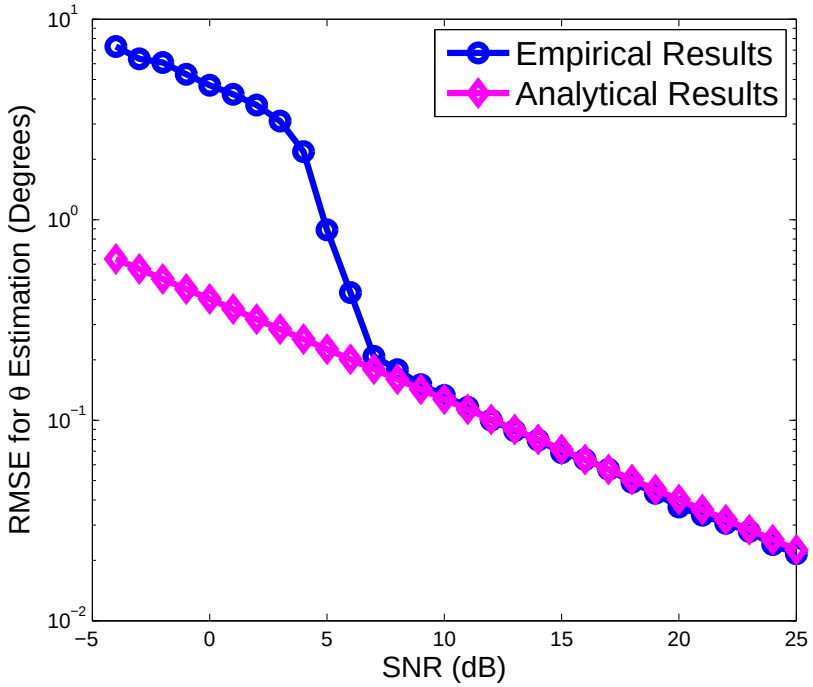

Figure 5.5: Elevation angle estimation for 16×4 array (Uniform DoA distribution).

the case of 16×16 antenna array, the RMSE estimation performance is shown in Figure 5.7 and 5.8. As expected, the 16×16 array outperforms the 8×8, 4×16 and 16×4 arrays in both elevation and azimuth angle estimation. It is to be emphasized here that these DoA estimation results hold for any continuous distribution, and is not specific to uniform distribution only. The results for 8×8 and 16×16 antenna arrays where the DoA's are drawn from Gaussian ($\mathcal{N}(50, 20)$) and exponential distribution ($Exp(1/50)$), are shown in comparing with Figures 5.1,5.2,5.7, and 5.8, we can clearly observe that for the same antenna

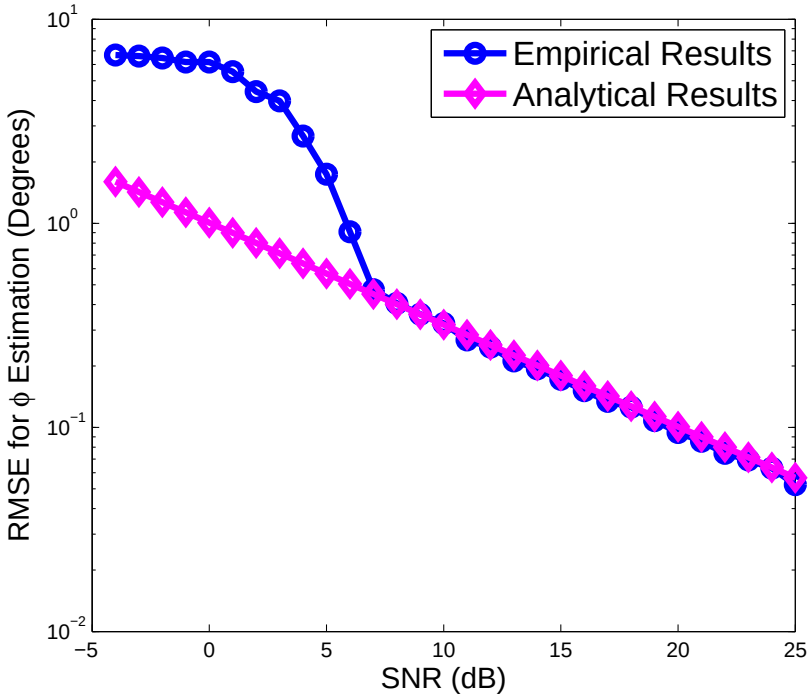

Figure 5.6: Azimuth angle estimation for 16×4 array (Uniform DoA distribution).

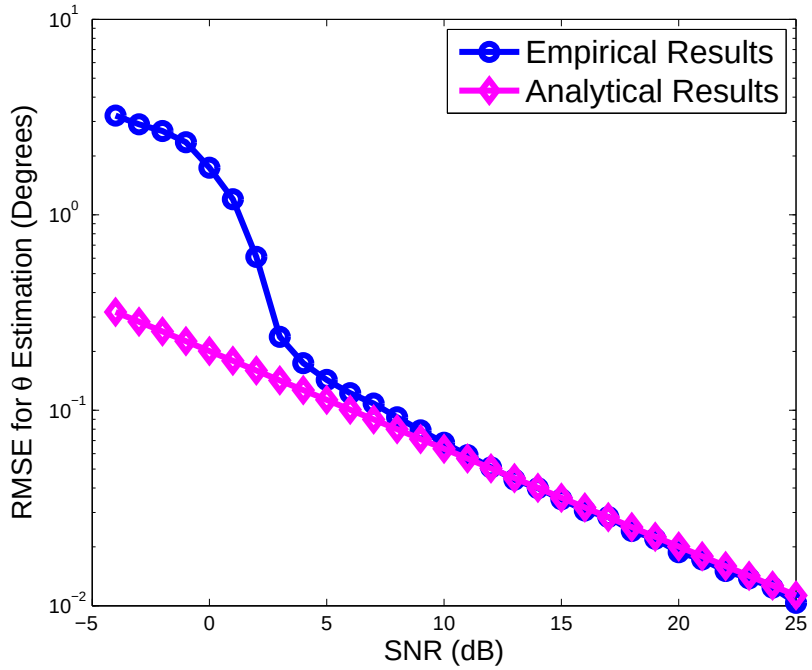

Figure 5.7: Elevation angle estimation for 16×16 array (Uniform DoA distribution).

configuration, the DoA estimation performance is very similar irrespective of the underlying distribution from which the DoA's are drawn. This, in fact, validates the results in Lemmas

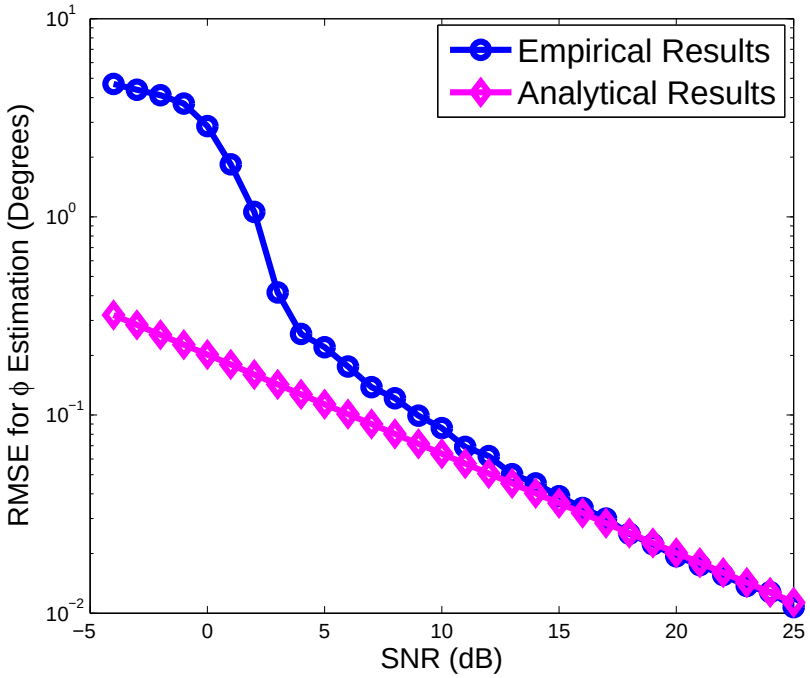

Figure 5.8: Azimuth angle estimation for 16×16 array (Uniform DoA distribution).

1 to 3.

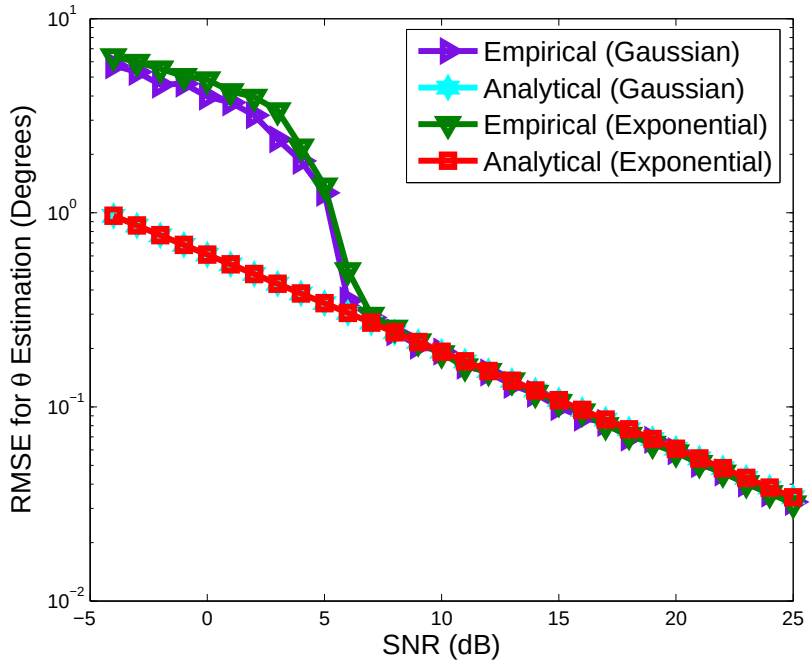

Figure 5.9: Elevation angle estimation for 8×8 array.

Figures that plot the RMSE of elevation and azimuth angles estimation as a function of

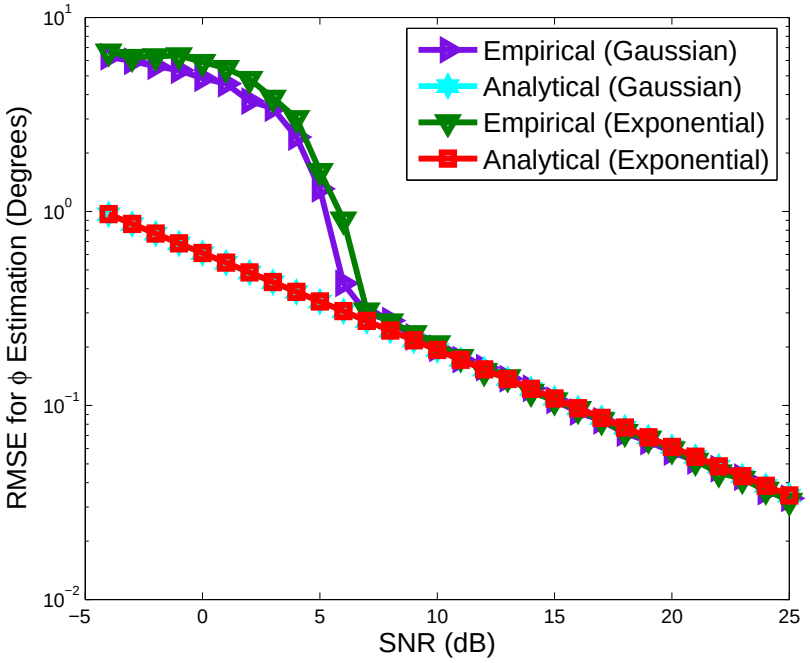

Figure 5.10: Azimuth angle estimation for 8×8 array.

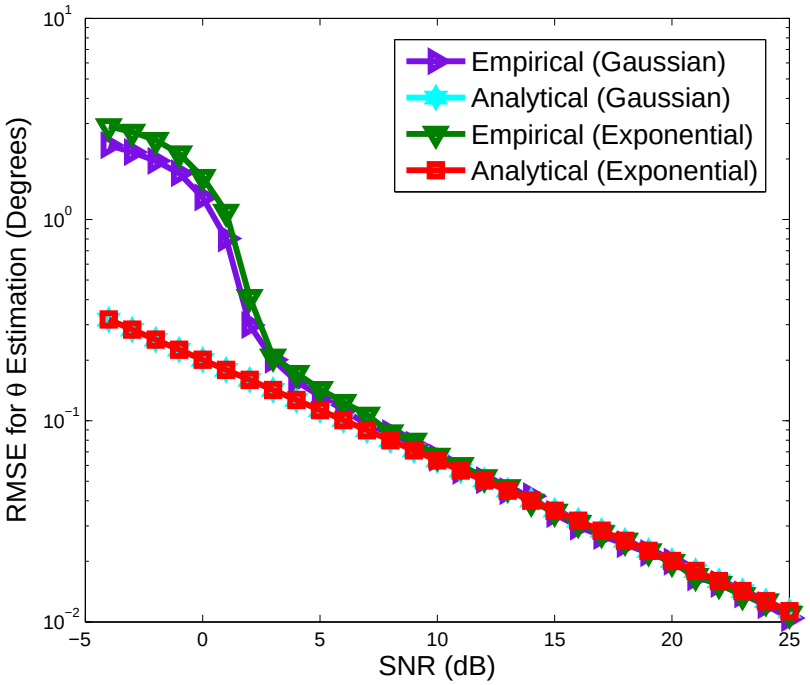

Figure 5.11: Elevation angle estimation for 16×16 array.

the number of antennas are shown in Figures 5.13 and 5.14 for uniform, Gaussian, and exponential DoA distributions, and SNR = 15 and 20 dB. Dashed lines represent the empirical

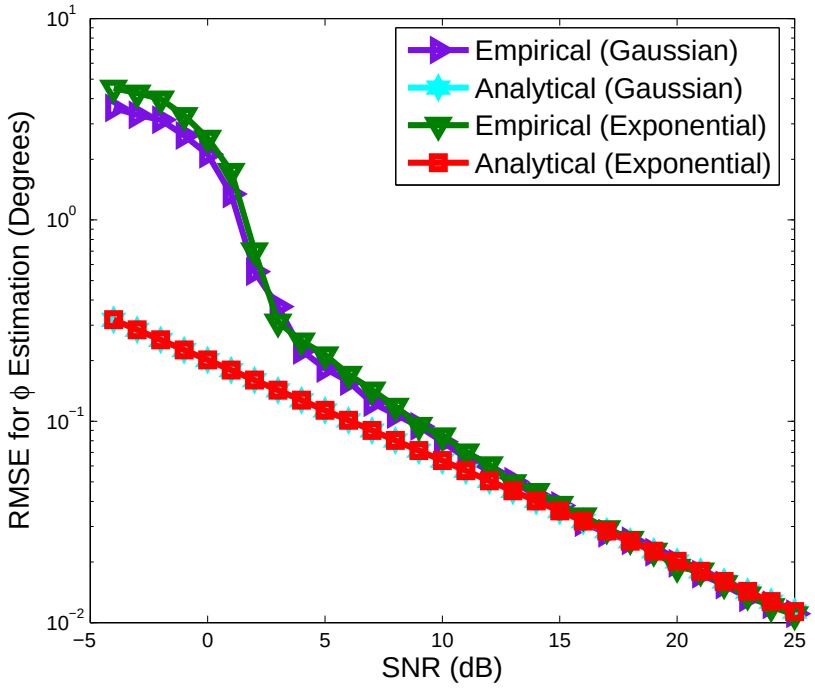

Figure 5.12: Azimuth angle estimation for 16×16 array.

results while solid lines represent the analytical results. The square array, where $M_1 = M_2$, is assumed for the evaluation. It can be observed that the DoA estimation performance improves as the number of antennas increases. Furthermore, in all cases, the empirical results are very close to the analytical results irrespective of the DoA distribution.

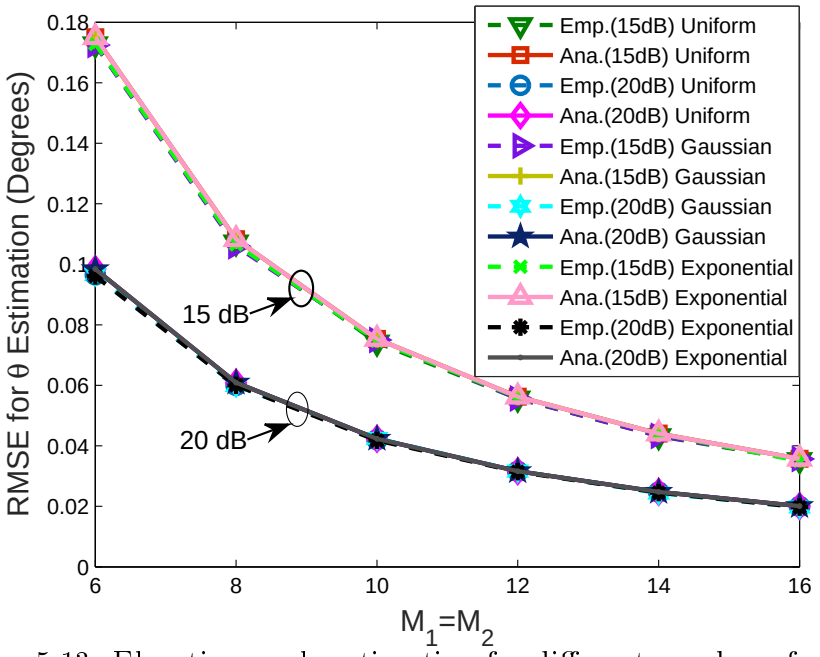

Figure 5.13: Elevation angle estimation for different number of antennas.

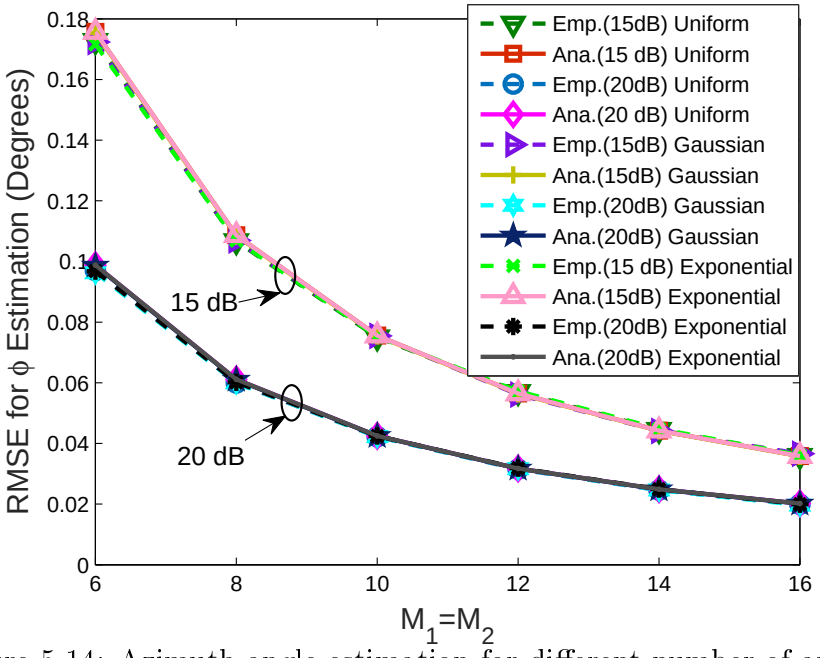

Figure 5.14: Azimuth angle estimation for different number of antennas.

Chapter 6

Conclusion

In this thesis, we have presented a DoA estimation procedure for the 3D massive-MIMO OFDM system. Specifically, we have derived the analytical expression of the root mean square estimation for the ESPRIT-type algorithms. Performance of elevation and azimuth angle estimation under various antenna configurations has been investigated. Results show that antenna configuration can play a vital role in determining the performance of the 3D massive-MIMO OFDM systems. Moreover, the correlation between the data on different sub-carriers has adverse effect on the DoA estimation Performance. This may provide significant intuition toward designing real massive-MIMO OFDM systems in future.

Appendix A

Appendix

A.1 Proof of Lemma 1

Proof. For any $i \neq m$,

$$[\bar{\mathbf{e}}_r(i)]^H[\bar{\mathbf{e}}_r(m)] = \frac{1}{N_r}\left[\mathbf{a}(v_i) \otimes \mathbf{a}(u_i)\right]^H \left[\mathbf{a}(v_m) \otimes \mathbf{a}(u_m)\right]$$

$$\begin{aligned}
&= \frac{1}{N_r}[1, e^{-ju_i}, \ldots, e^{-j(M_1-1)u_i}, \ldots, e^{-j(M_2-1)v_i} \qquad e^{-j(M_2-1)v_i}e^{-ju_i}, \ldots, e^{-j(M_2-1)v_i}e^{-j(M_1-1)u_i}] \\
&\quad [1, e^{ju_m}, \ldots, e^{j(M_1-1)u_m}, \ldots, e^{j(M_2-1)v_m} \qquad e^{j(M_2-1)v_m}e^{ju_m}, \ldots, e^{j(M_2-1)v_m}e^{j(M_1-1)u_m}]^T \\
&= \frac{1}{N_r}[1 + e^{-j(u_i-u_m)} +, \ldots, +e^{-j(M_1-1)(u_i-u_m)} +, \ldots, +e^{-j(M_2-1)(v_i-v_m)} \\
&+ e^{-j(M_2-1)(v_i-v_m)}e^{-j(u_i-u_m)} +, \ldots, \ldots, +e^{-j(M_2-1)(v_i-v_m)}e^{-j(M_1-1)(u_i-u_m)}] \qquad \text{(A.1)} \\
&= \frac{1}{N_r}\sum_{n=0}^{M_2-1}\sum_{p=0}^{M_1-1}[e^{-j(v_i-v_m)}]^n[e^{-j(u_i-u_m)}]^p \qquad \text{(A.2)}
\end{aligned}$$

Since both azimuth and elevation DoA's are drawn independently from a continuous distribution, $(v_i - v_m \neq 0)$ with probability = 1; therefore $e^{-j(v_i-v_m)} \neq 1$. Similarly, $e^{-j(u_i-u_m)} \neq 1$.

We can write,

$$\begin{aligned}
&\lim_{N_r\to\infty} \left|[\bar{\mathbf{e}}_r(i,k)]^H[\bar{\mathbf{e}}_r(j,k)]\right| \\
&= \lim_{N_r\to\infty} \frac{1}{N_r}\left|\sum_{n=0}^{M_2-1}\sum_{p=0}^{M_1-1}[e^{-j(v_i-v_m)}]^n[e^{-j(u_i-u_m)}]^p\right| \\
&\overset{a}{=} \lim_{N_r\to\infty} \frac{1}{N_r}\left|\frac{1-e^{-j(u_i-u_m)M_1}}{1-e^{-j(u_i-u_m)}}\right|\left|\frac{1-e^{-j(v_i-v_m)M_2}}{1-e^{-j(v_i-v_m)}}\right| \\
&\leq \lim_{N_r\to\infty} \frac{1}{N_r}\left|\frac{2}{1-e^{-j(u_i-u_m)}}\right|\left|\frac{2}{1-e^{-j(v_i-v_m)}}\right| = 0
\end{aligned} \tag{A.3}$$

where, (a) follows by noticing that both $\sum_{n=0}^{M_2-1}[e^{-j(v_i-v_m)}]^n$ and $\sum_{p=0}^{M_1-1}[e^{-j(u_i-u_m)}]^p$ form geometric series with the ratios $e^{-j(v_i-v_m)}$ and $e^{-j(u_i-u_m)}$, respectively. □

A.2 Proof of Theorem 1

Proof. In the case of standard ESPRIT and for circularly symmetric white noise, $\mathbf{C}_{nn} = \mathbf{0}$ [Roemer et al., 2014]. So, we can write (4.1) and (4.4) as

$$E\{(\Delta v_\ell)^2\} = \frac{1}{2}({\mathbf{r}_\ell^{(v)}}^H \mathbf{W}_{mat}^* \mathbf{R}_{nn}^T \mathbf{W}_{mat}^T \mathbf{r}_\ell^{(v)}), \tag{A.4}$$

$$E\{(\Delta u_\ell)^2\} = \frac{1}{2}({\mathbf{r}_\ell^{(u)}}^H \mathbf{W}_{mat}^* \mathbf{R}_{nn}^T \mathbf{W}_{mat}^T \mathbf{r}_\ell^{(u)}). \tag{A.5}$$

Let us now denote

$$\boldsymbol{\beta_\ell} = \mathbf{V_s}\boldsymbol{\Sigma_s^{-1}}\mathbf{q_\ell}, \tag{A.6}$$

$$\boldsymbol{\alpha_{v,\ell}} = (\mathbf{p_\ell^T}(\tilde{\mathbf{J}}_\mathbf{1}^{(v)}\mathbf{U_s})^+(\tilde{\mathbf{J}}_\mathbf{2}^{(v)}/e^{jv_\ell} - \tilde{\mathbf{J}}_\mathbf{1}^{(v)})(\mathbf{U_n}\mathbf{U_n^H}))^\mathbf{T}, \tag{A.7}$$

$$\boldsymbol{\alpha_{u,\ell}} = (\mathbf{p_\ell^T}(\tilde{\mathbf{J}}_\mathbf{1}^{(u)}\mathbf{U_s})^+(\tilde{\mathbf{J}}_\mathbf{2}^{(u)}/e^{ju_\ell} - \tilde{\mathbf{J}}_\mathbf{1}^{(u)})(\mathbf{U_n}\mathbf{U_n^H}))^\mathbf{T}. \tag{A.8}$$

So, we can have

$$\begin{aligned}\mathbf{W}_{mat}^{T}\mathbf{r}_{\ell}^{(v)} &= \left((\boldsymbol{\Sigma}_s^{-1}\mathbf{V}_s^T)\otimes(\mathbf{U}_n\mathbf{U}_n^H)\right)^T\left(\mathbf{q}_\ell\otimes\left(\left[(\tilde{\mathbf{J}}_1^{(v)}\mathbf{U}_s)^+(\tilde{\mathbf{J}}_2^{(v)}/e^{jv_\ell}-\mathbf{J}_1^{(v)})\right]^T\mathbf{p}_\ell\right)\right)\\ &= \left(\mathbf{V}_s\boldsymbol{\Sigma}_s^{-1}\mathbf{q}_\ell\right)\quad\otimes\left(\mathbf{p}_\ell^T(\tilde{\mathbf{J}}_1^{(v)}\mathbf{U}_s)^+\left(\tilde{\mathbf{J}}_2^{(v)}/e^{jv_\ell}-\mathbf{J}_1^{(v)}\right)\left(\mathbf{U}_n\mathbf{U}_n^H\right)\right)^T\\ &= \boldsymbol{\beta_\ell}\otimes\boldsymbol{\alpha_{v,\ell}}. \end{aligned}\tag{A.9}$$

Similarly, $\mathbf{W}_{mat}^{T}\mathbf{r}_{\ell}^{(u)} = \boldsymbol{\beta}_\ell\otimes\boldsymbol{\alpha}_{u,\ell}$. The MSE in (A.4) and (A.5) then can be expressed as

$$E\{(\Delta v_\ell)^2\} = \frac{1}{2}((\boldsymbol{\beta_\ell}\otimes\boldsymbol{\alpha_{v,\ell}})^H\mathbf{R}_{nn}^T(\boldsymbol{\beta_\ell}\otimes\boldsymbol{\alpha_{v,l}})),\tag{A.10}$$

$$E\{(\Delta u_\ell)^2\} = \frac{1}{2}((\boldsymbol{\beta_\ell}\otimes\boldsymbol{\alpha_{u,\ell}})^H\mathbf{R}_{nn}^T(\boldsymbol{\beta_\ell}\otimes\boldsymbol{\alpha_{u,\ell}})).\tag{A.11}$$

It can be easily verified that $\boldsymbol{\alpha}_{v,l}$ can be written as $\boldsymbol{\alpha}_{v,l}^T = \mathbf{c}_\ell^T\left(\left(\tilde{\mathbf{J}}_{v,2}\mathbf{A}\right)^+\tilde{\mathbf{J}}_{v,2}-\left(\tilde{\mathbf{J}}_{v,1}\mathbf{A}\right)^+\tilde{\mathbf{J}}_{v,1}\right)$; where $\mathbf{c}_\ell = [0,\ldots,1,\ldots 0]^T$ is the column selection vector with ℓ-th element being one, and other elements being zero, $\tilde{\mathbf{J}}_{v,1} = \mathbf{I}_{M_1}\otimes[\mathbf{I}_{M_2-1}\quad\mathbf{0}]$ and $\tilde{\mathbf{J}}_{v,2} = \mathbf{I}_{M_1}\otimes[\mathbf{0}\quad\mathbf{I}_{M_2-1}]$ are the selection matrices. The pseudo inverse of the selected signal can be significantly simplified as follows:

$$\begin{aligned}\left(\tilde{\mathbf{J}}_{v,1}\mathbf{A}\right)^+ &= \left(\left(\tilde{\mathbf{J}}_{v,1}\mathbf{A}\right)^H(\mathbf{J}_{v,1}\mathbf{A})\right)^{-1}\left(\tilde{\mathbf{J}}_{v,1}\mathbf{A}\right)^H\\ &= \frac{1}{(M_2-1)M_1}\left(\frac{\left(\tilde{\mathbf{J}}_{v,1}\mathbf{A}\right)^H\left(\tilde{\mathbf{J}}_{v,1}\mathbf{A}\right)}{(M_2-1)M_1}\right)^{-1}\left(\tilde{\mathbf{J}}_{v,1}\mathbf{A}\right)^H\\ &\overset{(a)}{=} \frac{1}{(M_2-1)M_1}\left(\tilde{\mathbf{J}}_{v,1}\mathbf{A}\right)^H,\end{aligned}\tag{A.12}$$

where (a) holds due to **Lemma** 1. Similarly, we have

$$\left(\tilde{\mathbf{J}}_{v,2}\mathbf{A}\right)^+ = \frac{1}{(M_2-1)M_1}\left(\tilde{\mathbf{J}}_{v,2}\mathbf{A}\right)^H.\tag{A.13}$$

In the same way, $\boldsymbol{\alpha}_{u,l}$ can be written as $\boldsymbol{\alpha}_{u,l}^T = \mathbf{c}_\ell^T \left(\left(\tilde{\mathbf{J}}_{u,2}\mathbf{A} \right)^+ \tilde{\mathbf{J}}_{u,2} - \left(\tilde{\mathbf{J}}_{u,1}\mathbf{A} \right)^+ \tilde{\mathbf{J}}_{u,1} \right)$; where $\tilde{\mathbf{J}}_{u,1} = [\mathbf{I}_{M_1-1} \quad \mathbf{0}] \otimes \mathbf{I}_{M_2}$ and $\tilde{\mathbf{J}}_{u,2} = [\mathbf{0} \quad \mathbf{I}_{M_1-1}] \otimes \mathbf{I}_{M_2}$ are the selection matrices. Therefore, we can have

$$\left(\tilde{\mathbf{J}}_{u,1}\mathbf{A} \right)^+ = \frac{1}{(M_1-1)M_2} \left(\tilde{\mathbf{J}}_{u,1}\mathbf{A} \right)^H, \tag{A.14}$$

$$\left(\tilde{\mathbf{J}}_{u,2}\mathbf{A} \right)^+ = \frac{1}{(M_1-1)M_2} \left(\tilde{\mathbf{J}}_{u,2}\mathbf{A} \right)^H. \tag{A.15}$$

Now,

$$\tilde{\mathbf{J}}_{v,1} = \begin{bmatrix} 1 & 0 & \dots & 0 \\ 0 & 1 & \dots & 0 \\ \vdots & \vdots & \ddots & \vdots \\ 0 & 0 & \dots & 1 \end{bmatrix}_{M_1 \times M_1} \otimes \begin{bmatrix} 1 & 0 & \dots & 0 & 0 \\ 0 & 1 & \dots & 0 & 0 \\ \vdots & \vdots & \ddots & \vdots & \vdots \\ 0 & 0 & \dots & 1 & 0 \end{bmatrix}_{M_2-1 \times M_2} \tag{A.16}$$

The ℓ-th row of $\left(\tilde{\mathbf{J}}_{v,1}\mathbf{A} \right)^H$ thus can be written as

$$\left[1, e^{-ju_\ell}, \dots, e^{-j(M_2-2)u_\ell}, \dots, e^{-j(M_2-1)v_\ell} e^{-j(M_1-1)u_\ell} \right].$$

Accordingly, ℓ-th row of $\left(\tilde{\mathbf{J}}_{v,1}\mathbf{A} \right)^H \tilde{\mathbf{J}}_{v,1}$ can be written as

$$\begin{aligned} &\mathbf{c}_\ell^T \left(\left(\tilde{\mathbf{J}}_{v,1}\mathbf{A} \right)^H \tilde{\mathbf{J}}_{v,1} \right) \\ &= \left[1, e^{-ju_\ell}, \dots, e^{-j(M_2-2)u_\ell}, \dots, e^{-j(M_2-1)v_\ell} e^{-j(M_1-2)u_\ell}, 0 \right]. \end{aligned} \tag{A.17}$$

Moreover, $\tilde{\mathbf{J}}_{v,2}$ can be represented as

$$\tilde{\mathbf{J}}_{v,2} = \begin{bmatrix} 1 & 0 & \dots & 0 \\ 0 & 1 & \dots & 0 \\ \vdots & \vdots & \ddots & \vdots \\ 0 & 0 & \dots & 1 \end{bmatrix}_{M_1 \times M_1} \otimes \begin{bmatrix} 0 & 1 & 0 & \dots & 0 \\ 0 & 0 & 1 & \dots & 0 \\ \vdots & \vdots & \vdots & \ddots & \vdots \\ 0 & 0 & 0 & \dots & 1 \end{bmatrix}_{M_2-1 \times M_2} \tag{A.18}$$

The ℓ-th row of $\left(\tilde{\mathbf{J}}_{v,2}\mathbf{A}\right)^H$ then can be written as

$$\left[e^{-ju_\ell}, e^{-j2u_\ell}, \ldots, e^{-j(M_2-1)u_\ell}, \ldots, e^{-j(M_2-1)v_\ell}e^{-j(M_1-1)u_\ell}\right],$$

and the ℓ-th row of $\left(\tilde{\mathbf{J}}_{v,2}\mathbf{A}\right)^H \tilde{\mathbf{J}}_{v,1}$ can be expressed as

$$\begin{aligned}
&\mathbf{c}_\ell^T \left(\left(\tilde{\mathbf{J}}_{v,2}\mathbf{A}\right)^H \tilde{\mathbf{J}}_{v,2}\right) \\
&= \left[0, e^{-ju_\ell}, \ldots, e^{-j(M_2-1)u_\ell}, \ldots, e^{-j(M_2-1)v_\ell}e^{-j(M_1-1)u_\ell}, 0\right]. \qquad \text{(A.19)}
\end{aligned}$$

Combining (A.17) and (A.19), we can obtain

$$\begin{aligned}
&\mathbf{c}_\ell^T \left(\left(\tilde{\mathbf{J}}_{v,2}\mathbf{A}\right)^H \tilde{\mathbf{J}}_{v,2} - \left(\tilde{\mathbf{J}}_{v,1}\mathbf{A}\right)^H \tilde{\mathbf{J}}_{v,1}\right) \\
&= \Big[-1, 0, \ldots, 0, e^{-j((M_2-1)u_\ell)}, \ldots, e^{-j((M_1-1)u_\ell)}, 0, \\
&\quad , \ldots, e^{-j((M_2-1)v_\ell+(M_1-1)u_\ell)}\Big]. \qquad \text{(A.20)}
\end{aligned}$$

Accordingly, we obtain $||\boldsymbol{\alpha}_{v,\ell}||^2 = 2/(M_2-1)^2M_1$. Following the same procedure, we can also have $||\boldsymbol{\alpha}_{u,\ell}||^2 = 2/(M_1-1)^2M_2$. With a view to deriving the expression for $\boldsymbol{\beta_\ell}$, we first rewrite the singular value decomposition of the forward-backward averaged noiseless received signal as:

$$\begin{aligned}
&\left[\mathbf{A}\text{diag}\{\mathbf{b}\}\tilde{\mathbf{E}}_t\tilde{\mathbf{S}} \quad \boldsymbol{\Pi}_{N_r}\mathbf{A}^*\text{diag}\{\mathbf{b}\}\tilde{\mathbf{E}}_t^*\tilde{\mathbf{S}}^*\boldsymbol{\Pi}_V\right] \\
&= \left[\mathbf{A}\text{diag}\{\mathbf{b}\}\tilde{\mathbf{E}}_t\tilde{\mathbf{S}} \quad \mathbf{A}\boldsymbol{\Lambda}\text{diag}\{\mathbf{b}\}\tilde{\mathbf{E}}_t^*\tilde{\mathbf{S}}^*\boldsymbol{\Pi}_V\right] \\
&= \mathbf{A}\text{diag}\{\mathbf{b}\}\left[\tilde{\mathbf{E}}_t\tilde{\mathbf{S}} \quad \boldsymbol{\Lambda}\tilde{\mathbf{E}}_t^*\tilde{\mathbf{S}}^*\boldsymbol{\Pi}_V\right], \qquad \text{(A.21)}
\end{aligned}$$

where

$$\boldsymbol{\Lambda} = \text{diag}\{[e^{-j((M_1-1)u_n+(M_2-1)v_n)}, \ldots, , \ldots, e^{-j((M_1-1)u_{(n-N_c+1)}+(M_2-1)v_{(n-N_c+1)})}]\}.$$

Comparing with (3.2), and based on **Lemma** 1, we have $\mathbf{U}_s = 1/\sqrt{N_r}\mathbf{A}$, $\mathbf{\Sigma}_s = \sqrt{2N_rV}\text{diag}\{\mathbf{b}\}$, and $\mathbf{V}_s^H = 1/\sqrt{2V}\begin{bmatrix}\tilde{\mathbf{E}}_t\tilde{\mathbf{S}} & \mathbf{\Lambda}\tilde{\mathbf{E}}_t^*\tilde{\mathbf{S}}^*\mathbf{\Pi}_V\end{bmatrix}$. The vector, $\boldsymbol{\beta_\ell}$ is given by $\boldsymbol{\beta_\ell} = \mathbf{V}_s\Sigma_s^{-1}\mathbf{U}_s^H\mathbf{A}\mathbf{c}_\ell$ [Li et al., 1993]. It can be shown that the unitary trransformation does not affect the MSE of the ESPRIT method [Roemer, 2012]. However, the statistics of the noise and signal subspace are changed when preprocessing like forward-backward averaging is applied. Now, the noise covariance matrix can be written as:

$$\mathbf{R}_{nn} = \mathbf{E}\{\text{vec}\{\mathbf{W}\}\text{vec}\{\mathbf{W}\}^H\}. \tag{A.22}$$

However, if the noise is assumed to be circularly symmetric and white Gaussian, we have $\mathbf{R}_{nn} = \sigma^2\mathbf{I}_{N_rV}$. Therefore

$$\begin{aligned}(\boldsymbol{\beta_\ell}\otimes\boldsymbol{\alpha_{v,\ell}})^H\mathbf{R}_{nn}^T(\boldsymbol{\beta_\ell}\otimes\boldsymbol{\alpha_{v,\ell}}) &= \sigma^2(\boldsymbol{\beta_\ell}\otimes\boldsymbol{\alpha_{v,\ell}})^H(\boldsymbol{\beta_\ell}\otimes\boldsymbol{\alpha_{v,\ell}})\\ &= \sigma^2(\boldsymbol{\beta}_\ell^H\boldsymbol{\beta_\ell})\otimes(\boldsymbol{\alpha}_{v,\ell}^H\boldsymbol{\alpha}_{v,\ell}).\end{aligned} \tag{A.23}$$

Since $\boldsymbol{\beta_\ell}$ is the ℓ-th column of $\mathbf{V}_s\Sigma_s^{-1}\mathbf{U}_s^H\mathbf{A}$, $||\boldsymbol{\beta_\ell}||^2$ is the ℓ-th diagonal element of $\mathbf{A}^H\mathbf{U}_s\mathbf{\Sigma}_s^{-2}\mathbf{U}_s^H\mathbf{A}$, which we can write as $||\boldsymbol{\beta}_\ell||^2 = \mathbf{R}_{SS}^{-1}(\ell,\ell)/V$ [Li et al., 1993], [Liu et al., 2014], where $\mathbf{R}_{SS}(\ell,\ell)$ is the ℓ-th diagonal element of the equivalent transmit signal covariance matrix. Plugging the value of $||\boldsymbol{\beta}_\ell||^2$ and $||\boldsymbol{\alpha}_{v,\ell}||^2$ in (A.23):

$$(\boldsymbol{\beta_\ell}\otimes\boldsymbol{\alpha_{v,\ell}})^H\mathbf{R}_{nn}^T(\boldsymbol{\beta_\ell}\otimes\boldsymbol{\alpha_{v,\ell}}) = \sigma^2\frac{\mathbf{R}_{SS}^{-1}(\ell,\ell)}{V}\frac{2}{(M_2-1)^2M_1}. \tag{A.24}$$

Similarly, we also have

$$(\boldsymbol{\beta_\ell}\otimes\boldsymbol{\alpha_{u,\ell}})^H\mathbf{R}_{nn}^T(\boldsymbol{\beta_\ell}\otimes\boldsymbol{\alpha_{u,\ell}}) = \sigma^2\frac{\mathbf{R}_{SS}^{-1}(\ell,\ell)}{V}\frac{2}{(M_1-1)^2M_2}. \tag{A.25}$$

Plugging the expression from (A.24) into (A.10) we get

$$E\{(\Delta v_\ell)^2\} = \frac{\mathbf{R}_{SS}^{-1}(\ell,\ell)}{V}\frac{\sigma^2}{(M_2-1)^2M_1}. \tag{A.26}$$

Similarly, by plugging the expression from (A.25) into (A.11):

$$E\{(\Delta u_\ell)^2\} = \frac{\mathbf{R}_{SS}^{-1}(\ell,\ell)}{V} \frac{\sigma^{\mathbf{2}}}{(M_1-1)^2 M_2}. \tag{A.27}$$

Based on Jacobian matrix, we have:

$$\mathbb{E}\left\{(\triangle\theta_\ell)^2\right\} = \mathbb{E}\left\{(\triangle u_\ell)^2\right\} \frac{1}{\pi^2 \sin^2(\theta_\ell)}, \tag{A.28}$$

$$\begin{aligned}\mathbb{E}\left\{(\triangle\phi_\ell)^2\right\} = &\frac{\mathbb{E}\left\{(\triangle u_\ell)^2\right\} \cot^2(\theta_\ell)\cot^2(\phi_\ell)}{\pi^2 \sin^2(\theta_\ell)} \\ &+ \frac{\mathbb{E}\left\{(\triangle v_\ell)^2\right\}}{\pi^2 \sin^2(\theta_\ell)\sin^2(\phi_\ell)}.\end{aligned} \tag{A.29}$$

Recognizing that $\text{RMSE}\{\theta_\ell\} = \sqrt{\mathbb{E}\{(\triangle\theta_\ell)^2\}}$ and $\text{RMSE}\{\phi_\ell\} = \sqrt{\mathbb{E}\{(\triangle\phi_\ell)^2\}}$, by substituting (A.26) and (A.27) into (A.28) and (A.29), respectively, we obtain the desired results. □

Bibliography

[El Ayach et al., 2012] El Ayach, O., Heath, R., Abu-Surra, S., Rajagopal, S., & Pi, Z. (2012). The capacity optimality of beam steering in large millimeter wave MIMO systems. In *IEEE Signal Processing Advances in Wireless Commun. (SPAWC), 2012* (pp. 100–104).

[Haardt et al., 2008] Haardt, M., Roemer, F., & Del Galdo, G. (2008). Higher-order SVD-based subspace estimation to improve the parameter estimation accuracy in multidimensional harmonic retrieval problems. *IEEE Trans. Signal Process.*, 56(7), 3198–3213.

[Larsen et al., 2009] Larsen, M., Swindlehurst, A., & Svantesson, T. (2009). Performance bounds for MIMO-OFDM channel estimation. *IEEE Trans. Signal Process.*, 57(5), 1901–1916.

[Larsson et al., 2014] Larsson, E., Edfors, O., Tufvesson, F., & Marzetta, T. (2014). Massive MIMO for next generation wireless systems. *IEEE Commun. Mag.*, 52(2), 186–195.

[Li et al., 1993] Li, F., Liu, H., & Vaccaro, R. (1993). Performance analysis for DoA estimation algorithms: unification, simplification, and observations. *IEEE Trans. Aerosp. Electron. Syst.*, 29(4), 1170–1184.

[Liu et al., 2014] Liu, L., Li, Y., & Zhang, J. (2014). DoA estimation and achievable rate analysis for 3D millimeter wave massive MIMO systems. In *IEEE Signal Processing Advances in Wireless Communications (SPAWC), 2014* (pp. 6–10).

[Mathews et al., 1996] Mathews, C. P., Haardt, M., & Zoltowski, M. (1996). Performance analysis of closed-form, ESPRIT based 2-D angle estimator for rectangular arrays. *IEEE Signal Process. Lett.*, 3(4), 124–126.

[Rangan et al., 2014] Rangan, S., Rappaport, T., & Erkip, E. (2014). Millimeter Wave Cellular Wireless Networks: Potentials and Challenges. *Proc. IEEE*, 102(3), 366–385.

[Roemer, 2012] Roemer, F. (2012). Advanced algebraic concept for efficient multi-channel signal processing. Doctoral Thesis.

[Roemer et al., 2014] Roemer, F., Haardt, M., & Del Galdo, G. (2014). Analytical performance assessment of multi-dimensional matrix- and tensor-based ESPRIT-type algorithms. *IEEE Trans. Signal Process.*, 62(10), 2611–2625.

[Sayeed & Sivanadyan, 2010] Sayeed, A. & Sivanadyan, T. (2010). *Handbook on Array Processing the Sensor Network*, chapter Wireless communication and sensing in multipath environments using multi-antenna transceivers. Wiley.

[Stuber et al., 2004] Stuber, G., Barry, J., McLaughlin, S., Li, Y., Ingram, M., & Pratt, T. (2004). Broadband MIMO-OFDM wireless communications. *Proceedings of the IEEE*, 92(2), 271–294.

[Wang et al., 2012] Wang, A., Liu, L., & Zhang, J. (2012). Low complexity direction of arrival (DoA) estimation for 2D massive MIMO systems. In *Globecom Workshops (GC Wkshps), 2012 IEEE* (pp. 703–707).